

# Geometry of River Networks III: Characterization of Component Connectivity

Peter Sheridan Dodds\*

*Department of Mathematics and Department of Earth, Atmospheric and Planetary Sciences,  
Massachusetts Institute of Technology, Cambridge, MA 02139.*

Daniel H. Rothman†

*Department of Earth, Atmospheric and Planetary Sciences,  
Massachusetts Institute of Technology, Cambridge, MA 02139.*

(Dated: October 27, 2018)

River networks serve as a paradigmatic example of all branching networks. Essential to understanding the overall structure of river networks is a knowledge of their detailed architecture. Here we show that sub-branches are distributed exponentially in size and that they are randomly distributed in space, thereby completely characterizing the most basic level of river network description. Specifically, an averaged view of network architecture is first provided by a proposed self-similarity statement about the scaling of drainage density, a local measure of stream concentration. This scaling of drainage density is shown to imply Tokunaga's law, a description of the scaling of side branch abundance along a given stream, as well as a scaling law for stream lengths. This establishes the scaling of the length scale associated with drainage density as the basic signature of self-similarity in river networks. We then consider fluctuations in drainage density and consequently the numbers of side branches. Data is analyzed for the Mississippi River basin and a model of random directed networks. Numbers of side streams are found to follow exponential distributions as are stream lengths and inter-tributary distances along streams. Finally, we derive the joint variation of side stream abundance with stream length, affording a full description of fluctuations in network structure. Fluctuations in side stream numbers are shown to be a direct result of fluctuations in stream lengths. This is the last paper in a series of three on the geometry of river networks.

PACS numbers: 64.60.Ht, 92.40.Fb, 92.40.Gc, 68.70.+w

## I. INTRODUCTION

This is the last paper in a series of three on the geometry of river networks. In the first [1] we examine in detail the description of river networks by scaling laws [2, 3, 4, 5] and the evidence for universality. Additional introductory remarks concerning the motivation of the overall work are to found in this first paper. In the second article [6] we address distributions of the basic components of river networks, stream segments and sub-networks. Here, we provide an analysis complementary to the work of the second paper by establishing a description of how river network components fit together. As before, we are motivated by the premise that while relationships of mean quantities are primary in any investigation, the behavior of higher order moments potentially and often do encode significant information.

Our purpose then is to investigate the distributions of quantities which describe the architecture of river networks. The goal is to quantify these distributions and, where this is not possible, to quantify fluctuations. In particular, we center our attention on Tokunaga's law [7, 8, 9] which is a statement about network architec-

ture describing the tributary structure of streams. Since Tokunaga's law can be seen as the main part of a platform from which all other river network scaling laws follow [4], it is an obvious starting point for the investigation of fluctuations in river network structure. We use data from the Schediegger model of random networks [10] and the Mississippi river. We find the distributions obtained from these two disparate sources agree very well in form. We are able to write down scaling forms of all distributions studied. We observe a number of distributions to be exponential, therefore requiring only one parameter for their description. As a result, we introduce a dimensionless scale  $\xi_t$ , finding it to be sufficient to describe the fluctuations present in Tokunaga's law and thus potentially all river network scaling laws. Significantly, we observe the spatial distribution of stream segments to be random implying we have reached the most basic description of network architecture.

Tokunaga's law is also intimately connected with drainage density,  $\rho$ , a quantity which will be used throughout the paper. Drainage density is a measure of stream concentration or, equivalently, how a network fills space. We explore this connection in detail, showing how simple assumptions regarding drainage density lead to Tokunaga's law.

The paper is structured as follows. We first outline Horton-Strahler stream ordering which provides the necessary descriptive taxonomy for river network architecture. We then define Tokunaga's law and introduce a

---

\*Author to whom correspondence should be addressed; Electronic address: dodds@segovia.mit.edu; URL: <http://segovia.mit.edu/>

†Electronic address: dan@segovia.mit.edu

scaling law for a specific form of drainage density. We briefly describe Horton’s laws for stream number and length and some simple variations. (Both stream ordering and Horton’s laws are covered in more detail in [6]). We show that the scaling law of drainage density may be taken as an assumption from which all other scaling laws follow. We also briefly consider the variation of basin shapes (basin allometry) in the context of directedness. This brings us to the focal point of the paper, the identification of a statistical generalization of Tokunaga’s law. We first examine distributions of numbers of tributaries (side streams) and compare these with distributions of stream segment lengths. We observe both distributions to be exponential leading to the notion that stream segments are distributed randomly throughout a network. The presence of exponential distributions also leads to the introduction of the characteristic number  $\xi_t$  and the single length-scale  $\xi_{l^{(s)}} \propto \xi_t$ . We then study the variation of tributary spacing along streams so as to understand fluctuations in drainage density and again find the signature of randomness. This leads us to develop a joint probability distribution connecting the length of a stream with the frequency of its side streams.

## II. DEFINITIONS

### A. Stream ordering

Horton-Strahler stream ordering[11, 12] breaks a river network down into a set of *stream segments*. The method can be thought of as an iterative pruning. First, we define a *source stream* as the stream section that runs from a channel head to the first junction with another stream. These source streams are classified as the *first-order* stream segments of the network. Next, we remove all source streams and identify the new source streams of the remaining network. These are the network’s *second-order* stream segments. The process is repeated until one stream segment is left of order  $\Omega$ . The order of the basin is then defined to be  $\Omega$  (we will use the words basin and network interchangeably).

In discussing network architecture, we will speak of *side streams* and *absorbing streams*. A side stream is any stream that joins into a stream of higher order, the latter being the absorbing stream. We will denote the orders of absorbing and side streams by  $\mu$  and  $\nu$  but when referring to an isolated stream or streams where their relative rank is ambiguous, we will write stream order as  $\omega$ , subscripted as seems appealing.

Central to our investigation of network architecture is stream segment length. As in [6], we denote this length by  $l_\omega^{(s)}$  for a stream segment of order  $\omega$ . We will also introduce a number of closely related lengths which describe distances between side streams. When referring to streams throughout we will specifically mean stream segments of a particular order unless otherwise indicated. This is to avoid confusion with the natural definition of a

stream which is the path from a point on a network moving upstream to the most distant source. For an order  $\omega$  basin, we denote this *main stream length* by  $l_\omega$

Note also that we consider river networks in planform, i.e., as networks projected onto the horizontal (or gravitationally flat) plane. This simplification poses no great concern for the analysis of large scale networks such as the Mississippi but must be considered in the context of drainage basins with significant relief.

### B. Tokunaga’s law

Defining a stream ordering on a network allows for a number of well-defined measures of connectivity, stream lengths and drainage areas. Around a decade after the Strahler-improved stream ordering of Horton appeared, Tokunaga introduced the idea of measuring side stream statistics [7, 8, 9]. This technique arguably provides the most useful measurement based on stream ordering but has only recently received much attention [4, 13, 14, 15]. The idea is simply, for a given network, to count the average number of order  $\nu$  side streams entering an order  $\mu$  absorbing stream. This gives  $\langle T_{\mu,\nu} \rangle$ , a set of double-indexed parameters for a basin. Note that  $\Omega \geq \mu > \nu \geq 1$ , so we can view the Tokunaga ratios as a lower triangular matrix. An example for the Mississippi river is shown in Table I [30] The same data is represented pictorially in Figure 1 in what we refer to as a *Tokunaga graph*.

	$\nu = 1$	2	3	4	5	6	7	8	9	10
$\mu = 2$	1.7									
3	4.9	1.3								
4	12	3.8	1.1							
5	29	9.1	2.9	1.0						
6	71	23	7.7	3.0	1.2					
7	190	56	19	7.8	3.3	1.1				
8	380	110	39	17	6.9	2.6	1.0			
9	630	170	64	28	11	4.5	3.0	0.60		
10	1100	270	66	29	13	4.3	2.7	1	1	
11	1400	510	120	66	25	12	9	3	1	1

TABLE I: Tokunaga ratios for the Mississippi River. The row indices are the absorbing stream orders while the columns correspond to side stream orders. Each entry is the average number of order  $\nu$  side streams per order  $\mu$  absorbing stream.

Tokunaga made several key observations about these side stream ratios. The first is that because of the self-similar nature of river networks, the  $\langle T_{\mu,\nu} \rangle$  should not depend absolutely on either of  $\mu$  or  $\nu$  but only on the relative difference, i.e.,  $k = \mu - \nu$ . The second is that in changing the value of  $k = \mu - \nu$ , the  $\langle T_{\mu,\nu} \rangle$  must themselves change by a systematic ratio. These statements

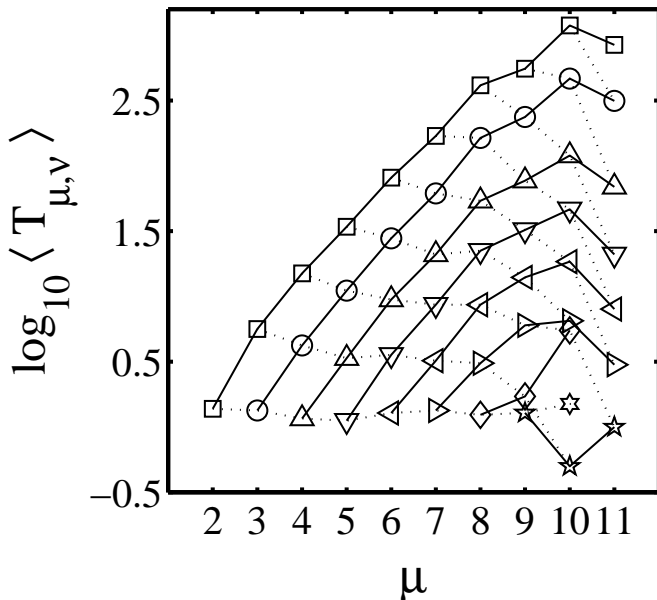


FIG. 1: A Tokunaga graph for the Mississippi River. The values are given in Table I. Each point represents a Tokunaga ratio  $\langle T_{\mu,\nu} \rangle$ . The solid lines follow variations in the order of the absorbing stream  $\mu$  while the dotted lines follow unit increments in both  $\mu$  and  $\nu$ , the order of side streams. In comparison, the Tokunaga graph of an exactly self-similar network would have points evenly spaced at  $\ln T_1 + (\mu + \nu - 1) \ln R_T$  where  $1 \leq \nu < \mu = 2, 3, \dots, \Omega$ , i.e., all lines in the plot would be straight and uniformly spaced, with the dotted lines being horizontal. The nature of deviations in scalings laws for river networks is addressed in [1].

lead to Tokunaga's law:

$$\langle T_{\mu,\nu} \rangle = \langle T_k \rangle = \langle T_1 \rangle (R_T)^{k-1}. \quad (1)$$

Thus, only two parameters are necessary to characterize the set of  $T_{\mu,\nu}$ :  $T_1$  and  $R_T$ .

The parameter  $T_1 > 0$  is the average number of side streams of one order lower than the absorbing stream, typically on the order of 1.0–1.5. Since these side streams of one order less are the dominant side streams of the basin, their number estimates the basin's breadth. In general, larger values of  $\langle T_1 \rangle$  correspond to wider basins while smaller values are in keeping with basins with relatively thinner profiles.

The ratio  $R_T > 1$  measures how the density of side streams of decreasing order increases. It is a measure of changing length scales and has a simple interpretation with respect to Horton's laws which we describe below. Thus, already inherent in Tokunaga's law is a generalization of drainage density  $\rho$ , the usual definition of which is given as follows. For a given region of landscape with area  $A$  with streams totalling in length  $L$ ,  $\rho = L/A$  and has the dimensions of an inverse length scale [11]. One may think of  $\rho$  as the inverse of the typical distance between

streams, i.e., the characteristic scale beyond which erosion cannot more finely dissect the landscape [11]. In principle, drainage density may vary from landscape to landscape and also throughout a single region. Below, we will turn this observation about Tokunaga's law around to show that all river network scaling laws may be derived from an expanded notion of drainage density.

Even though the number of side streams entering any absorbing stream must of course be an integer, Tokunaga's ratios are under no similar obligation since they are averages. Nevertheless, Tokunaga's law provides a good sense of the structure of a network albeit at a level of averages. One of our main objectives here is to go further and consider fluctuations about and the full distributions underlying the  $\langle T_{\mu,\nu} \rangle$ .

Finally, a third important observation of Tokunaga is that two of Horton's laws follow from Tokunaga's law, which we next discuss.

### C. Horton's laws

We review Horton's laws [4, 11, 16] and then show how self-similarity and drainage density lead to Tokunaga's law, Horton's laws and hence all other river network scaling laws.

The relevant quantities for Horton's relations are  $n_\omega$ , the number of order  $\omega$  streams, and  $\langle l_\omega \rangle$ , the average main stream length (as opposed to stream segment length  $\langle l_\omega^{(s)} \rangle$ ) of order  $\omega$  basins. The laws are simply that the ratio of these quantities from order to order remain constant:

$$\frac{n_{\omega+1}}{n_\omega} = 1/R_n \quad \text{and} \quad \frac{\langle l_{\omega+1} \rangle}{\langle l_\omega \rangle} = R_l, \quad (2)$$

for  $\omega \geq 1$ . Note the definitions are chosen so that all ratios are greater than unity. The number of streams decreases with order while all areas and lengths grow.

A similar law for basin areas [11, 16] states that  $\langle a_{\omega+1} \rangle / \langle a_\omega \rangle = R_a$  where  $\langle a_\omega \rangle$  is the average drainage area of an order  $\omega$  basin. However, with the assumption of uniform drainage density it can be shown that  $R_n \equiv R_a$  [4] so we are left with the two independent Horton laws of equation (2).

As in [6], we consider another Horton-like law for stream segment lengths:

$$\frac{\langle l_{\omega+1}^{(s)} \rangle}{\langle l_\omega^{(s)} \rangle} = R_{l^{(s)}}. \quad (3)$$

As we will show, the form of the distribution of the variable  $T_{\mu,\nu}$  is a direct consequence of the distribution of  $l_\omega^{(s)}$ .

Tokunaga showed that Horton's laws of stream number and stream length follow from what we have called Tokunaga's law, equation (1). For example, the solution of a difference equation relating the  $n_\omega$  and the  $T_k$

leads to the result  $R_n = A_T + [A_T^2 - 2R_T]^{1/2}$  where  $A_T = (2 + R_T + T_1)/2$  for  $\Omega = \infty$  and a more complicated expression is obtained for finite  $\Omega$  [4, 8, 9, 15]. In keeping with our previous remarks on  $T_1$ , this expression for  $R_n$  shows that an increase in  $T_1$  will increase  $R_n$  which, since  $R_a \equiv R_n$ , corresponds to a network where basins tend to be relatively broader. Our considerations will expand significantly on this connection between the network descriptions of Horton and Tokunaga.

### III. THE IMPLICATIONS OF A SCALING LAW FOR DRAINAGE DENSITY

We now introduce a law for drainage density based on stream ordering. We write  $\rho_{\mu,\nu}$  for the number of side streams of order  $\nu$  per unit length of order  $\mu$  absorbing stream. We expect these densities to be independent of the order of the absorbing stream and so we will generally use  $\rho_\nu$ . The typical length separating order  $\nu$  side streams is then  $1/\rho_\nu$ . Assuming self-similarity of river networks, we must have

$$\rho_{\nu+1}/\rho_\nu = 1/R_\rho \quad (4)$$

where  $R_\rho > 1$  independent of  $\nu$ .

All river network scaling laws in the planform may be seen to follow from this relationship. Consider an absorbing stream of order  $\mu$ . Self-similarity immediately demands that the number of side streams of order  $\mu - 1$  must be statistically independent of  $\mu$ . This number is of course  $\langle T_1 \rangle$ . Therefore, the typical length of an order  $\mu$  absorbing stream must be

$$\langle l_\mu^{(s)} \rangle = \langle T_1 \rangle / \rho_{\mu-1}. \quad (5)$$

Using equation (4) to replace  $\rho_{\mu-1}$  in the above equation, we find

$$T_1/\rho_{\mu-1} = R_\rho T_1/\rho_{\mu-2}. \quad (6)$$

Thus,  $T_2 = R_\rho T_1$  and, in general  $T_k = (R_\rho)^{k-1} T_1$ . This is Tokunaga's law and we therefore have

$$R_\rho \equiv R_T. \quad (7)$$

Equation (4) and equation (5) also give

$$\langle l_\mu^{(s)} \rangle = T_1/\rho_{\mu-1} = R_\rho T_1/\rho_{\mu-2} = R_\rho \langle l_{\mu-1}^{(s)} \rangle. \quad (8)$$

On comparison with equation (3), we see that the above is our Hortonian law of stream segment lengths and that

$$R_\rho \equiv R_{l^{(s)}}. \quad (9)$$

As  $R_{l^{(s)}}$  is the basic length-scale ratio in the problem, we rewrite equation (4), our Hortonian law of drainage density, as

$$\rho_{\nu+1}/\rho_\nu = 1/R_{l^{(s)}}. \quad (10)$$

The above statement becomes our definition of the self-similarity of drainage density.

### IV. BASIN ALLOMETRY

Given that we have suggested the need for only a single relevant length ratio, we must remark here on basin allometry. Allometry refers to the relative growth or scaling of a shape's dimensions and was originally introduced in the context of biology [17]. A growth or change being allometric usually implies it is not self-similar. A long-standing issue in the study of river networks has been whether or not basins are allometric [3, 5, 18].

Consider two basins described by  $(L_1, W_1)$  and  $(L_2, W_2)$  within the same system where  $L_i$  is a characteristic longitudinal basin length and  $W_i$  a characteristic width. The basins being allometric means that  $(W_1/W_2) = (L_1/L_2)^H$  where  $H < 1$ . Thus, two length ratios are needed to describe the allometry of basins. If we consider basins defined by stream ordering then we have the Horton-like ratios  $R_L$  and  $R_W = R_L^H$ . Now, when rescaling an entire basin, streams roughly aligned with a basin's length will rescale with the factor  $R_L$  and those perpendicular to the basin's axis will rescale differently with  $R_W$ . This creates a conundrum: how can basins be allometric ( $R_L \neq R_W$ ) and yet individual streams be self-similar ( $R_L = R_W$ ) as implied by Horton's laws?

We contend the answer is that allometry must be restricted to *directed networks* and that self-similarity of basins must hold for *non-directed networks*. This is in agreement with Colaiori *et al.* [19] who also distinguish between self-similar and allometric river basins although we stress here the qualification of directedness. Directed networks have a global direction of flow in which the direction of each individual stream flow has a positive component. A basic example is the random model of Scheidegger [10] which we describe below. For a directed network,  $R_L = R_l$ , and the rescaling of basin sizes matches up with the rescaling of stream lengths regardless of how the basin's width rescales since all streams are on average aligned with the global direction of flow. Hence, our premise that streams rescale in a self-similar way is general enough to deal with systems whose basins rescale in an allometric fashion.

In considering the allometry of basins, we must also address the additional possibility that individual stream lengths may scale non-trivially with basin length. In this case, the main stream length  $l$  would vary with the longitudinal basin length  $L$  as  $l \propto L^d$ . This is typically a weak dependence with  $1.0 < d < 1.15$  [2, 20]. Note that Horton's laws still apply in this case. The exponent  $d$  plays a part in determining whether or not a basin scales allometrically. The exponent  $H$  introduced in the discussion of basin allometry can be found in terms of Horton's ratios (or equivalently Tokunaga's parameters) and  $d$  as  $H = d \ln R_n / \ln R_l - 1$  [4].

Thus, for a directed network  $d = 1$  and  $H \leq 1$  (e.g., Scheidegger [10]) whereas for undirected, self-similar networks  $H = 1$  and  $d \geq 1$  (e.g., random undirected networks [21, 22]). River networks are in practice often nei-

ther fully directed or undirected. Scaling laws observed in such cases will show deviations from pure scaling that may well be gradual and difficult to detect [1].

## V. TOKUNAGA DISTRIBUTIONS

The laws of Tokunaga and Horton relate averages of quantities. In the remainder of this paper, we investigate the underlying distributions from which these averages are made. We are able to find general scaling forms of a number of distributions and in many cases also identify the basic form of the relevant scaling function.

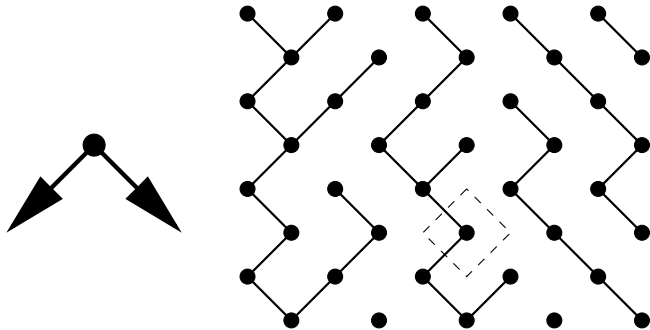


FIG. 2: Scheidegger's random directed networks. Sites are arranged on a triangular lattice and stream flow is directed down the page. At each site, the flow direction is randomly chosen to be in one of the directions shown on the left. The dashed box indicates the area "drained" by the local site.

To aid and motivate our investigations, we examine, as we have done in both [1] and [6], a simple model of directed random networks that was first introduced by Scheidegger [10]. Since we make much of use this model in the present work, we provide a self-contained discussion. Consider the triangular lattice of sites oriented as in Figure 2. At each site of the lattice a stream flow direction is randomly chosen between the two possible diagonal directions shown. It is therefore trivial to generate the model on a large scale, allowing for a thorough investigation of its river network statistics. The small, tilted box with a dashed boundary represents the area drained by the enclosed site. As with many discrete-space models, the details of the underlying lattice are unimportant. On a square lattice, the model's streams would have three choices of flow, two diagonals and straight down the page. However, the choice of a triangular lattice does simplify implementation and calculation of statistics. For example, only one tributary can exist at each site along a stream and stream paths and basin boundaries are precisely those of the usual discrete-space random walk [23].

Since random walks are well understood, the exponents of many river network scaling laws are exactly known for the Scheidegger model [24, 25, 26, 27] and analogies may also be drawn with the Abelian sandpile model [28]. For example, a basin's boundaries being random walks

means that a basin of length  $L$  will typically have a width  $W \propto L^{1/2}$  which gives  $H = 1/2$ . Since the network is directed, stream length is the same as basin length,  $l = L$ , so we trivially have  $d = 1$ . Basin area  $a$  is estimated by  $WL \propto L^{3/2} \propto l^{3/2}$  so  $l \propto a^{2/3}$  giving Hack's law with an exponent of  $2/3$  [18].

Nevertheless, the Tokunaga parameters and the Horton ratios are not known analytically. Estimates from previous work [4] find  $T_1 \simeq 1.35$ ,  $R_l = R_T \simeq 3.00$  and  $R_n \simeq 5.20$ . Data for the present analysis was obtained on  $L = 10^4$  by  $W = 3 \times 10^3$  lattices with periodic boundaries. Given the self-averaging present in any single instance on these networks, ensembles of 10 were deemed sufficient.

We first examine the distributions of Tokunaga ratios  $T_{\mu,\nu}$  and observe a strong link to the underlying distribution of  $l_\mu^{(s)}$ . Both are well described by exponential distributions. To understand this link, we next consider the distances between neighboring side streams of like order. This provides a measure of fluctuations in drainage density and again, exponential distributions appear. We are then in a position to develop theory for the joint probability distribution between the Tokunaga ratios and stream segment lengths and, as a result, the distribution for the quantity  $T_{\mu,\nu}/l_\mu^{(s)}$  and its inverse. In the limit of large  $\mu$ , the  $T_{\mu,\nu}$  are effectively proportional to  $l_\mu^{(s)}$  and all fluctuations of the former exactly follow those of the latter.

All investigations are initially carried out for the Scheidegger model where we may generate statistics of ever-improving quality. We find the same forms for all distributions for the Mississippi data (and for other river networks not presented here) and provide some pertinent examples. Perhaps the most significant benefit of the simple Scheidegger model is its ability to provide clean distributions whose form we can then search for in real data.

Figure 3 shows the distribution of the number of order  $\nu = 2$  side streams entering an order  $\mu = 6$  absorbing stream for the Scheidegger model. At first, it may seem surprising that this is not a single-peaked distribution centered around  $\langle T_{\mu,\nu} \rangle$  dying off for small and large values of  $T_{\mu,\nu}$ .

The distribution of  $T_{\mu,\nu}$  in Figure 3 is clearly well described by an exponential distribution. This can also be seen upon inspection of Figures 4(a) and 4(b). Figure 4(a) shows normalized distributions of  $T_{\mu,\nu}$  for  $\nu = 2$  and varying absorbing stream order  $\mu = 4, 5$  and  $6$ . These distributions (plus the one for absorbing stream order  $\mu = 7$ ) are rescaled and presented in Figure 4(b). The single form thus obtained suggests a scaling form of the  $T_{\mu,\nu}$  distribution is given by

$$P(T_{\mu,\nu}) = (R_{l^{(s)}})^{-\mu} F [T_{\mu,\nu} (R_{l^{(s)}})^{-\mu}]. \quad (11)$$

where  $F$  is an exponential scaling function. However, this only accounts for variations in  $\mu$ , the order of the absorbing stream.

Figures 5(a) and 5(b) show that a similar rescaling of the distributions may be effected when  $\nu$  is varied. In this

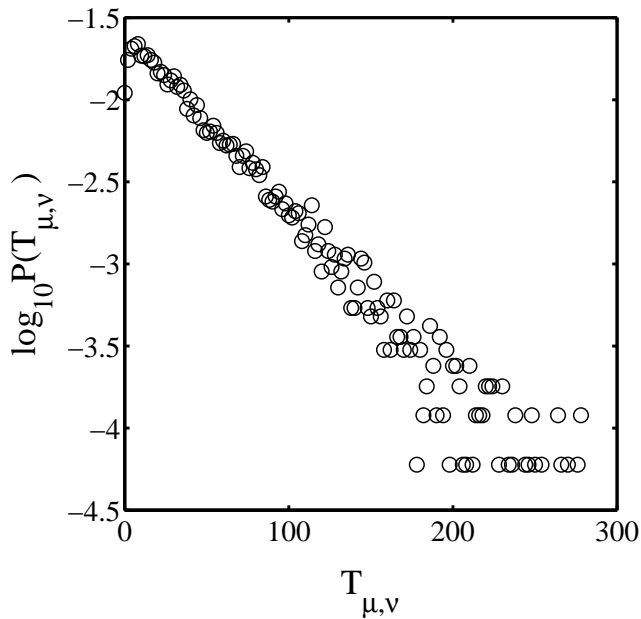


FIG. 3: An example of a generalized Tokunaga distribution for the Scheidegger model. The Tokunaga ratio  $T_{\mu,\nu}$  is the number of side streams of order  $\nu$  entering an absorbing stream of order  $\mu$ . For this particular example  $\mu = 6$  and  $\nu = 2$ . The form is exponential and is a result of variations in stream segment length rather than significant fluctuations in side stream density.

case, the data is for the Mississippi. The rescaling is now by  $R_{l^{(s)}}$  rather than  $R_{l^{(s)}}^{-1}$  and equation (11) is improved to give

$$P(T_{\mu,\nu}) = (R_{l^{(s)}})^{\mu-\nu-1} P_T [T_{\mu,\nu}/(R_{l^{(s)}})^{\mu-\nu-1}]. \quad (12)$$

The function  $P_T$  is a normalized exponential distribution independent of  $\mu$  and  $\nu$ ,

$$P_T(z) = \frac{1}{\xi_t} e^{-z/\xi_t}, \quad (13)$$

where  $\xi_t$  is the characteristic number of side streams of one order lower than the absorbing stream, i.e.,  $\xi_t = \langle T_1 \rangle$ . For the Mississippi, we observe  $\xi_t \simeq 1.1$  whereas for the Scheidegger model,  $\xi_t \simeq 1.35$ . As expected, the Tokunaga distribution is dependent only on  $k = \mu - \nu$  so we can write

$$P(T_k) = (R_{l^{(s)}})^{k-1} P_T [T_{\mu,\nu}/(R_{l^{(s)}})^{k-1}]. \quad (14)$$

with  $P_T$  as above.

## VI. DISTRIBUTIONS OF STREAM SEGMENT LENGTHS AND RANDOMNESS

As we have suggested, the distributions of the Tokunaga ratios depend strongly on the distributions of stream

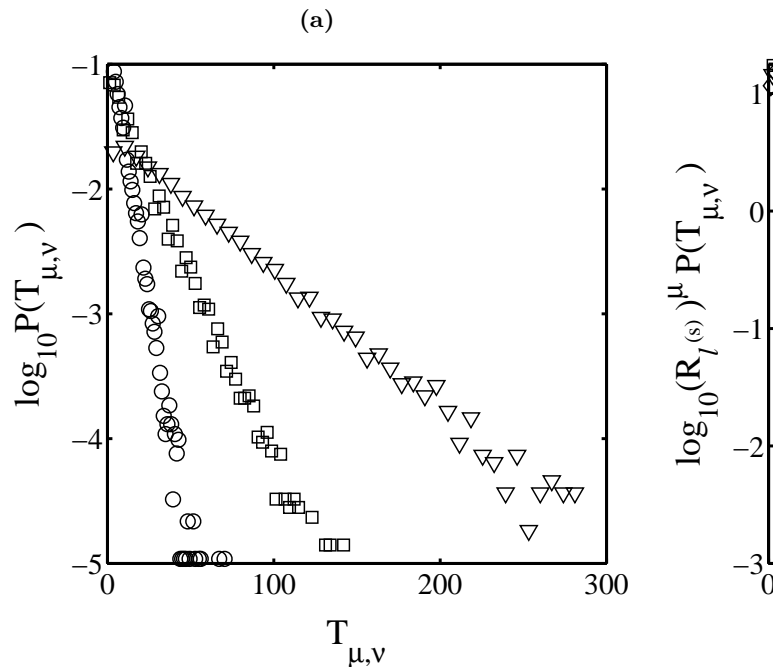


FIG. 4: Distributions for Tokunaga ratios for varying orders of absorbing stream and fixed side stream order of  $\nu = 2$  for the Scheidegger network. In (a), examples of  $T_{\mu,\nu}$  distributions for absorbing stream order  $\mu = 4$  (circles),  $\mu = 5$  (squares) and  $\mu = 6$  (triangles). In (b), these distributions, as well as the  $\mu = 7$  case, are rescaled according to equation (11). The resulting “data collapse” gives a single distribution. For the Scheidegger model,  $R_{l^{(s)}} \simeq 3.00$ .

segment lengths. Figure 6 indicates why this is so. The form of the underlying distribution is itself exponential. We have already examined this fact extensively in [6] and here we develop its relationship with the Tokunaga distributions.

Figures 6(a) and 6(b) show that the distributions of  $l_\mu^{(s)}$  can be rescaled in the same way as the Tokunaga distributions. Thus, we write the distribution for stream segment lengths as [6]

$$P(l_\mu^{(s)}) = (R_{l^{(s)}})^{-\mu+1} P_{l^{(s)}} [l_\mu^{(s)}/(R_{l^{(s)}})^{-\mu+1}]. \quad (15)$$

As for  $P_T$ , the function  $P_{l^{(s)}}$  is a normalized exponential distribution

$$P_{l^{(s)}}(z) = \frac{1}{\xi_{l^{(s)}}} e^{-z/\xi_{l^{(s)}}}, \quad (16)$$

where, in a strictly self-similar network,  $\xi_{l^{(s)}}$  is the characteristic length of first-order stream segments, i.e.,  $\xi_{l^{(s)}} = \langle l_1^{(s)} \rangle$ . (Note that in [6] we use  $\xi$  for  $\xi_{l^{(s)}}$  for ease of notation). We qualify this by requiring the network to be exactly self-similar because in most models and all real networks this is certainly not the case. As should be expected, there are deviations from scaling for the largest

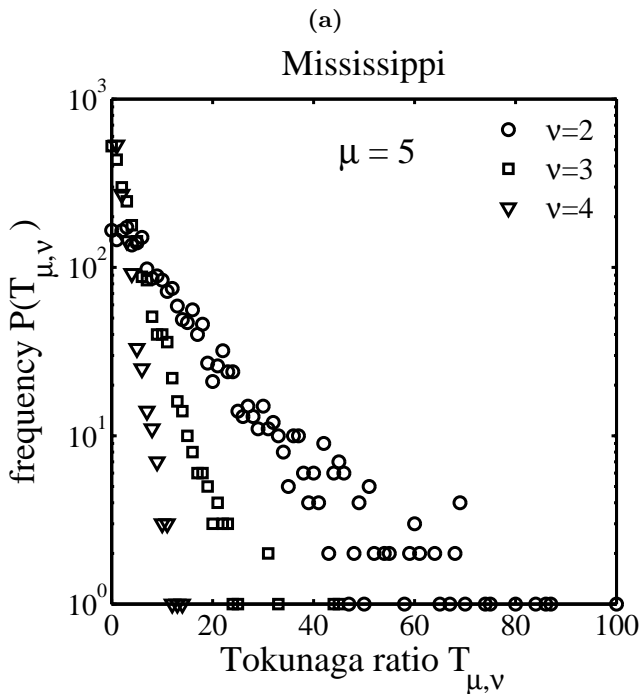


FIG. 5: Tokunaga distributions for varying side stream orders for the Mississippi river basin. In both (a) and (b), the absorbing stream order is  $\mu = 5$  and the side stream orders are  $\nu = 2$  (circles),  $\nu = 3$  (squares) and  $\nu = 4$  (triangles). The raw distributions are shown in (a). In (b) the distributions are rescaled as per equation (12). For the Mississippi, the ratio is estimated to be  $R_{l^{(s)}} \simeq 2.40$  [6].

and smallest orders. Therefore,  $\xi_{l^{(s)}}$  is the characteristic size of a first-order stream as determined by scaling down the average lengths of those higher order streams that are in the self-similar structure of the network. It is thus in general different from  $\langle l_1^{(s)} \rangle$ .

We therefore see that the distributions of  $T_{\mu,\nu}$  and  $l_\mu^{(s)}$  are both exponential in form. Variations in  $l_\mu^{(s)}$  largely govern the possible values of the  $T_{\mu,\nu}$ . However,  $T_{\mu,\nu}$  is still only proportional to  $l_\mu^{(s)}$  on average and later on we will explore the joint distribution from which these individual exponentials arise.

The connection between the characteristic number  $\xi_t$  and the length-scale  $\xi_{l^{(s)}}$  follows from equations (3), (5), and (10):

$$\xi_t = \rho_1 R_{l^{(s)}} \xi_{l^{(s)}}. \quad (17)$$

This presumes exact scaling of drainage densities and in the case where this is not so,  $\rho_1$  would be chosen so that  $(R_{l^{(s)}})^{\nu-1} \rho_1$  most closely approximates the higher order  $\rho_\nu$ .

We come to an important interpretation of the exponential distribution as a composition of independent probabilities. Consider the example of stream segment lengths. We write  $\tilde{p}_\mu$  as the probability that a stream

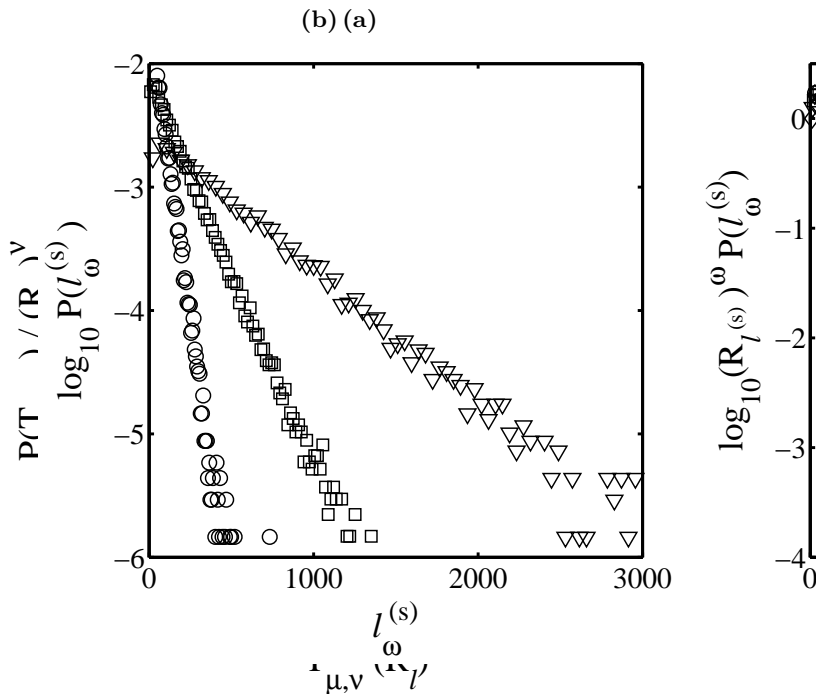


FIG. 6: Stream segment length distributions for varying stream order for the Scheidegger model. Lengths are in units the lattice spacing. Shown in (a) are raw distributions for  $\omega = 4$  (circles),  $\omega = 5$  (squares) and  $\omega = 6$ . The linear forms on the semilogarithmic axes indicate these distributions are well approximated by exponentials [6]. In (b), the distributions in (a) plus the distribution for  $l_7^{(s)}$  (diamonds) are rescaled using equation (15).

segment of order  $\mu$  meets with (and thereby terminates at) a stream of order at least  $\mu$ . For simplicity, we assume only one side stream or none may join a stream at any site. We also take the lattice spacing  $\alpha$  to be unity so that stream lengths are integers and therefore equate with the number of links between sites along a stream. For  $\alpha \neq 1$ , derivations similar to below will apply with  $l_\mu^{(s)}$  replaced by  $[l_\mu^{(s)}/\alpha]$ , where  $[\cdot]$  denotes rounding to the nearest integer. Note that extra complications arise when the distances between neighboring sites are not uniform.

Consider a single instance of an order  $\mu$  stream segment. The probability of this segment having a length  $l_\mu^{(s)}$  is given by

$$P(l_\mu^{(s)}) = \tilde{p}_\mu (1 - \tilde{p}_\mu)^{l_\mu^{(s)}}. \quad (18)$$

where  $\tilde{p}_\mu$  is the probability that an order  $\mu$  stream segment terminates on meeting a stream of equal or higher order. We can re-express the above equation as

$$P(l_\mu^{(s)}) \simeq \tilde{p}_\mu \exp\{-l_\mu^{(s)} \ln(1 - \tilde{p}_\mu)^{-1}\}, \quad (19)$$

and upon inspection of equations (15) and (16) we make the identification

$$(R_{l^{(s)}})^{\mu-1} \xi_{l^{(s)}} = [-\ln(1 - \tilde{p}_\mu)]^{-1}, \quad (20)$$

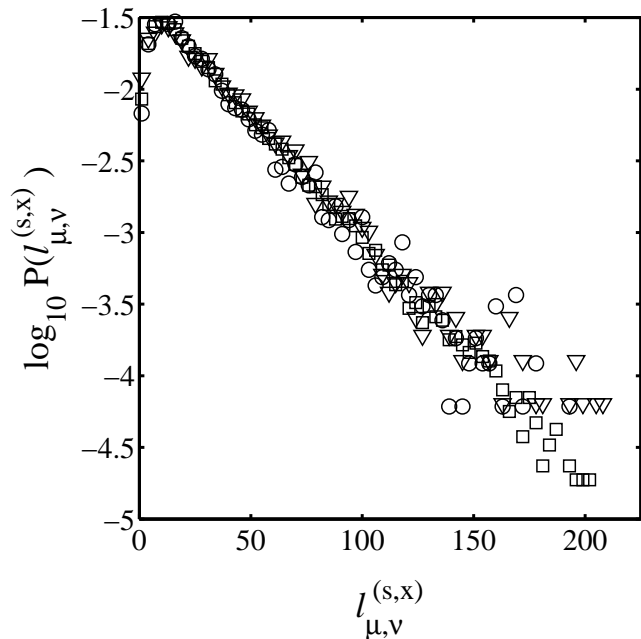


FIG. 7: A comparison of inter-tributary length distributions for the Scheidegger model. The example here is for order  $\mu = 6$  absorbing streams and order  $\nu = 3$  side streams. Note that no rescaling of the distributions has been performed. The three length variables here correspond to  $x=b$ ,  $x=i$  and  $x=e$ , i.e.,  $l_{\mu,\nu}^{(s,b)}$  (circles)  $l_{\mu,\nu}^{(s,i)}$  (squares), and  $l_{\mu,\nu}^{(s,e)}$  (triangles). These are the beginning, internal and end distances between entering side branches, defined fully in the text. No quantitative difference between these three lengths is observed.

which has the inversion

$$\tilde{p}_\mu = 1 - e^{-1/(R_{l^{(s)}})^{\mu-1} \xi_{l^{(s)}}}. \quad (21)$$

For  $\mu$  sufficiently large such that  $\tilde{p}_\mu \ll 1$ , we have the simplification

$$\tilde{p}_\mu \simeq 1/(R_{l^{(s)}})^{\mu-1} \xi_{l^{(s)}}. \quad (22)$$

We see that the probabilities satisfy the Horton-like scaling law

$$\tilde{p}_\mu / \tilde{p}_{\mu-1} = 1/R_{l^{(s)}}. \quad (23)$$

Thus, we begin to see the element of randomness in our expanded description of network architecture. The termination of a stream segment by meeting a larger branch is effectively a spatially random process.

## VII. GENERALIZED DRAINAGE DENSITY

Having observed the similarity of the distributions of  $T_{\mu,\nu}$  and  $l_\mu^{(s)}$ , we proceed to examine the exact nature of the relationship between the two. To do so, we introduce three new measures of stream length. These are  $l_{\mu,\nu}^{(s,b)}$ ,

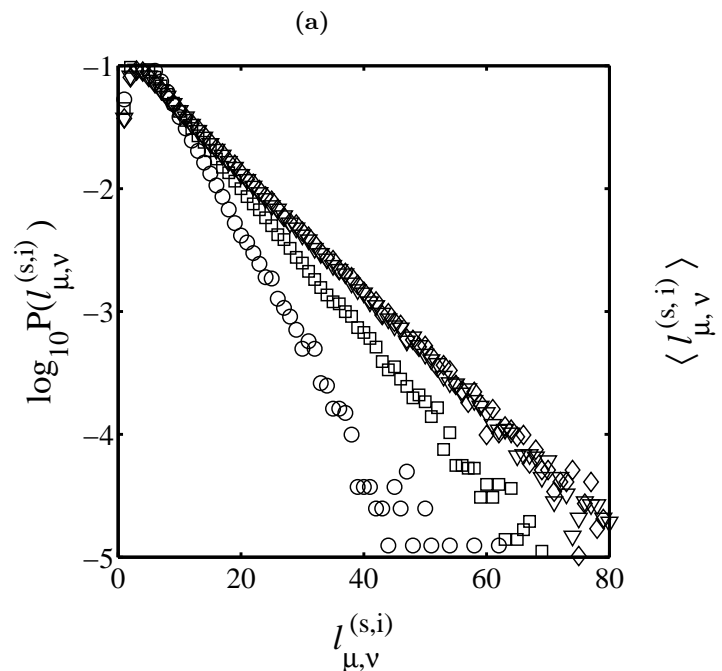


FIG. 8: An examination of the asymptotic behavior of distributions of internal inter-tributary lengths. The data here is for the Scheidegger model for the case of fixed side stream order  $\nu = 2$ . The plot in (a) shows distributions for absorbing stream order  $\mu = 3$  (circles),  $\mu = 4$  (squares),  $\mu = 6$  (triangles), and  $\mu = 8$  (diamonds). As  $\mu$  increases, the distributions, which are all individually exponential, tend towards a fixed exponential distribution. Since lower order stream segments have typically smaller lengths, they statistically block larger values of  $l_{\mu,\nu}^{(s,i)}$ , reducing the extent of the distribution tails for low  $\mu$ . This is further evidenced in (b) which provides a plot of  $\langle l_{\mu,\nu}^{(s,i)} \rangle$ , the mean inter-tributary stream length, as a function of  $\mu$  with  $\nu = 2$ . These mean values approach  $\langle l_{\mu,\nu=2}^{(s,i)} \rangle = 1/\rho_2 \simeq 10.1$  where  $\rho_2$  is the density of second-order side streams.

the distance from the beginning of an order  $\mu$  absorbing stream to the first order  $\nu$  side stream;  $l_{\mu,\nu}^{(s,i)}$ , the distance between any two adjacent internal order  $\nu$  side streams along an order  $\mu$  absorbing stream; and  $l_{\mu,\nu}^{(s,e)}$ , the distance from the last order  $\nu$  side stream to the end of an order  $\mu$  absorbing stream. By analysis of these inter-tributary lengths, we will be able to discern the distribution of side stream location along absorbing streams. This leads directly to a more general picture of drainage density which we fully expand upon in the following section.

Figure 7 compares normalized distributions of  $l_{\mu,\nu}^{(s,b)}$ ,  $l_{\mu,\nu}^{(s,i)}$  and  $l_{\mu,\nu}^{(s,e)}$  for the Scheidegger model. The data is for the distance between order  $\nu = 3$  side streams entering order  $\mu = 6$  absorbing streams. Once again, the distributions are well approximated by exponential distributions. Moreover, they are indistinguishable. This indicates, at least for the Scheidegger model, that drainage density is



independent of relative position of tributaries along an absorbing stream.

We now consider the effect on the distribution of inter-nal inter-tributary distances  $l_{\mu,\nu}^{(s,i)}$  following from variations in  $\mu$ , the order of the absorbing stream. Figure 8(a) provides a comparison of  $l_{\mu,\nu}^{(s,i)}$  distributions for  $\nu = 2$  and  $\mu = 3$  through  $\mu = 8$ . As  $\mu$  increases, the distributions tend towards a limiting function. With increasing  $\mu$  we are, on average, sampling absorbing streams of greater length and the full range of  $l_{\mu,\nu}^{(s,i)}$  becomes accordingly more accessible. This approach to a fixed distribution is reflected in the means of the distributions in Figure 8(a). Shown in Figure 8(b), the means  $\langle l_{\mu,\nu}^{(s,i)} \rangle$  for  $\nu = 2$  approach a value of around 10.1. The corresponding density of second-order streams for the Scheidegger model is thus  $\rho_2 = 1/\langle l_{\mu,\nu=2}^{(s,i)} \rangle \simeq 0.01$ . Higher drainage densities follow from equation (10). However, since deviations occur for small  $\nu$ , there will also be an approach to uniform scaling to consider with drainage density.

### VIII. JOINT VARIATION OF TOKUNAGA RATIOS AND STREAM SEGMENT LENGTH

We have so far observed that the individual distributions of the  $l_{\mu}^{(s)}$  and  $T_{\mu,\nu}$  are exponential and that they are related via the side-stream density  $\rho_n u$ . However, this is not an exact relationship. For example, given a collection of stream segments with a fixed length  $l_{\mu}^{(s)}$  we expect to find fluctuations in the corresponding Tokunaga ratios  $T_{\mu,\nu}$ .

To investigate this further we now consider the joint variation of  $T_{\mu,\nu}$  with  $l_{\mu}^{(s)}$  from a number of perspectives. After discussing the full joint probability distribution  $P(T_{\mu,\nu}, l_{\mu}^{(s)})$  we then focus on the quotient  $v = T_{\mu,\nu}/l_{\mu}^{(s)}$  and its reciprocal  $w = l_{\mu}^{(s)}/T_{\mu,\nu}$ . The latter two quantities are measures of drainage density and inter-tributary length for an individual absorbing stream.

#### A. The joint probability distribution

We build the joint distribution of  $P(T_{\mu,\nu}, l_{\mu}^{(s)})$  from our conception that stream segments are randomly distributed throughout a basin. In equation (18), we have the probability of a stream segment terminating after  $l_{\mu}^{(s)}$  steps. We need to incorporate into this form the probability that the stream segment also has  $T_{\mu,\nu}$  order  $\nu$  side streams. Since we assume placement of these side streams to be random, we modify equation (18) to find

$$P(l_{\mu}^{(s)}, T_{\mu,\nu}) = \tilde{p}_{\mu} \binom{l_{\mu}^{(s)} - 1}{T_{\mu,\nu}} p_{\nu}^{T_{\mu,\nu}} (1 - p_{\nu} - \tilde{p}_{\mu})^{l_{\mu}^{(s)} - T_{\mu,\nu} - 1}, \quad (24)$$

where  $\binom{n}{k} = n!/k!(n-k)!$  is the binomial coefficient and  $p_{\nu}$  is the probability of absorbing an order  $\nu$  side stream.

The extra  $p_{\nu}$  appears in the last factor  $(1 - p_{\nu} - \tilde{p}_{\mu})$  because this term is the probability that at a particular site the stream segment neither terminates nor absorbs an order  $\nu$  side stream. Also, it is simple to verify that the sum over  $l_{\mu}^{(s)}$  and  $T_{\mu,\nu}$  of the probability in equation (19) returns unity.

While equation (19) does precisely describe the joint distribution  $P(l_{\mu}^{(s)}, T_{\mu,\nu})$ , it is somewhat cumbersome to work with. We therefore find an analogous form defined for continuous rather than discrete variables. We simplify our notation by writing  $p = p_{\nu}$ ,  $q = (1 - p_{\nu} - \tilde{p}_{\mu})$  and  $\tilde{p} = \tilde{p}_{\mu}$ . We also replace  $(l_{\mu}^{(s)}, T_{\mu,\nu})$  by  $(x, y)$  where now  $x, y \in \mathbb{R}$ . Note that  $0 \leq y \leq x - 1$  since the number of side streams cannot be greater than the number of sites within a stream segment.

Equation (19) becomes

$$P(x, y) = N \tilde{p} \frac{\Gamma(x)}{\Gamma(y+1)\Gamma(x-y)} (p)^y (q)^{x-y-1}, \quad (25)$$

where we have used  $\Gamma(z+1) = z!$  to generalize the binomial coefficient. We have included the normalization  $N$  to account for the fact that we have moved to continuous variables and the resulting probability may not be cleanly normalized. Also we must allow that  $N = N(p, \tilde{p})$  and we will be able to identify this form more fully later on. Using Stirling's approximation [29], that  $\Gamma(z+1) \sim \sqrt{2\pi} z^{z+1/2} e^{-z}$ , we then have

$$\begin{aligned} P(x, y) &= N \tilde{p} p^y q^{x-y-1} \frac{1}{\sqrt{2\pi}} \frac{(x-1)^{x-3/2}}{y^{y+1/2} (x-y-1)^{x-y-1/2}} \\ &= N \frac{\tilde{p}}{\sqrt{2\pi} q} p^y q^{x-y} (x-1)^{-1/2} \left(\frac{y}{x-1}\right)^{-y-1/2} \left(1 - \frac{y}{x-1}\right)^{-1} \\ &\simeq N' x^{-1/2} [F(y/x)]^x \end{aligned}$$

where we have absorbed  $N$  and all terms involving only  $p$  and  $\tilde{p}$  into the prefactor  $N' = N'(p, \tilde{p}) = N \tilde{p}/(\sqrt{2\pi} q)$ . We have also assumed  $x$  is large such that  $x-1 \simeq x$  and  $1 \gg 1/x \simeq 0$ .

The function  $F(v) = F(v; p, q)$  identified above has the form

$$F(v) = \left(\frac{1-v}{q}\right)^{-(1-v)} \left(\frac{v}{p}\right)^{-v}. \quad (27)$$

where  $0 < v < 1$  (here and later, the variable  $v$  will refer to  $y/x$ ). Note that for fixed  $x$ , the conditional probability  $P(y|x)$  is proportional to  $[F(y/x)]^x$ . Figure 9(a) shows  $[F(v)]^x$  for a range of powers  $x$ . The basic function has a single peak situated near  $v = p$ . For increasing  $x$  which corresponds to increasing  $l_{\mu}^{(s)}$ , the peak becomes sharper approaching (when normalized) a delta function, i.e.,  $\lim_{x \rightarrow \infty} [F(v)]^x = \delta(v - p)$ .

Figure 9(b) provides a comparison between data for the Scheidegger model and the analytic form of  $P(l_{\mu}^{(s)}, T_{\mu,\nu})$ . For this example,  $\mu = 6$  and  $\nu = 2$  which corresponds to  $p \simeq 0.10$ ,  $q \simeq 0.90$  and  $\tilde{p} \simeq 0.001$  (using the results

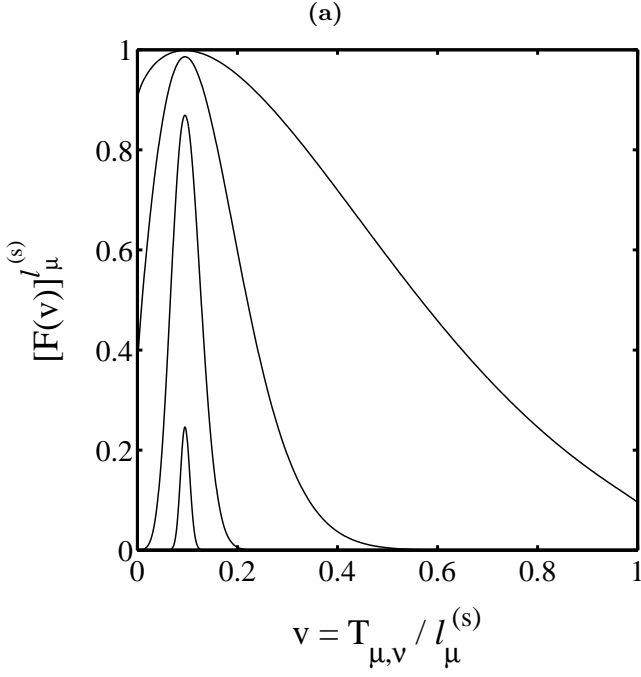


FIG. 9: Form of the joint distribution of Tokunaga ratios and stream segment lengths. The distribution is given in equation (26) and is built around the function  $F(v = T_{\mu,\nu}/l_\mu^{(s)})$  given in equation (27). Shown in (a) is  $[F(v)]^{l_\mu^{(s)}}$  for  $l_\mu^{(s)} = 1, 10, 100$  and  $1000$ . Increasing  $l_\mu^{(s)}$  corresponds to the focusing of the shape. In (b), the distribution  $P(T_{\mu,\nu} | l_\mu^{(s)} \simeq 340)$  is compared between theory (smooth curve) and data from the Scheidegger model (circles). The Scheidegger model data is compiled for a range of values of  $l_\mu^{(s)}$  rescaled as per equation (28).

of the previous section). The smooth curve shown is the conditional probability  $P(y | X)$  for the example value of  $X = l_\mu^{(s)} \simeq 340$  following from equation (26). From simulations, we obtain a discretized approximation to  $P(l_\mu^{(s)}, T_{\mu,\nu})$ . For each fixed  $x = l_\mu^{(s)}$  in the range  $165 \lesssim l_\mu^{(s)} \lesssim 345$ , we rescale the data using the following derived from equation (26),

$$P(X, y) = N' X^{-1/2} \left( N'^{-1} x^{1/2} P(x, y) \right)^{X/x}. \quad (28)$$

All rescaled data is then combined, binned and plotted as circles in Figure 9(b), showing excellent agreement with the theoretical curve.

### B. Distributions of side branches per unit stream length

Having obtained the general form of  $P(l_\mu^{(s)}, T_{\mu,\nu})$ , we now delve further into its properties by investigating the

distributions of the ratio  $w = T_{\mu,\nu}/l_\mu^{(s)}$  and its reciprocal  $1/w$ .

The quantity  $T_{\mu,\nu}/l_\mu^{(s)}$  is the number of side streams per length of a given absorbing stream and when averaged over an ensemble of absorbing streams gives

$$\langle T_{\mu,\nu}/l_\mu^{(s)} \rangle = \rho_\nu. \quad (29)$$

Accordingly, the reciprocal  $l_\mu^{(s)}/T_{\mu,\nu}$  is the average separation of side streams of order  $\nu$ .

First, we derive  $P(T_{\mu,\nu}/l_\mu^{(s)})$  from  $P(l_\mu^{(s)}, T_{\mu,\nu})$ . We then consider some intuitive rescalings which will allow us to reduce the form of the normalization  $N(p, q)$ .

We rewrite equation (26) as

$$P(x, y) = N' x^{-1/2} \exp \{ -x \ln [-F(y/x)] \}. \quad (30)$$

We transform  $(x, y)$  to the modified polar coordinate system described by  $(u, v)$  with the relations

$$u^2 = x^2 + y^2 = T_{\mu,\nu}^2 \text{ and } v = y/x. \quad (31)$$

The inverse relations are  $x = u/(1+v^2)$  and  $y = uv/(1+v^2)$  and we also have  $dx dy = x du dv$ . Equation (32) leads to

$$P(u, v) = N' \left( \frac{u}{1+v^2} \right)^{1/2} \exp \left\{ -\frac{u}{1+v^2} \ln [-F(v)] \right\}. \quad (32)$$

To find  $P(v)$  we integrate out over the radial dimension  $u$ :

$$\begin{aligned} P(v) &= \int_{u=0}^{\infty} du P(u, v) \\ &= N' \int_{u=0}^{\infty} du \left( \frac{u}{1+v^2} \right)^{1/2} \exp \left\{ -\frac{u}{1+v^2} \ln [-F(v)] \right\} \\ &= N' (1+v^2) (\ln [-F(v)])^{-3/2} \int_{z=0}^{\infty} dz z^{1/2} e^{-z} \\ &= N'' \frac{1+v^2}{(\ln [-F(v)])^{3/2}}. \end{aligned} \quad (33)$$

Here,  $N'' = N' \Gamma(3/2) = N' \sqrt{\pi}/2$  and we have used the substitution  $z = u/(1+v^2) \ln [-F(v)]$ .

The distribution for  $w = l_\mu^{(s)}/T_{\mu,\nu} = 1/v$  follows simply from equation (33) and we find

$$P(w) = N'' \frac{1+w^2}{w^4 (\ln [-F(1/w)])^{3/2}}. \quad (34)$$

Figures 10(a) and 10(b) compare the predicted forms of  $P(v)$  and  $P(w)$  with data from the Scheidegger model. In both cases, the data is for order  $\nu = 2$  side streams being absorbed by streams of order  $\mu = 6$ . Note that both distributions show an initially exponential-like decay away from a central peak. Moreover, the agreement is excellent, offering further support to the notion that the spatial distribution of stream segments is random.

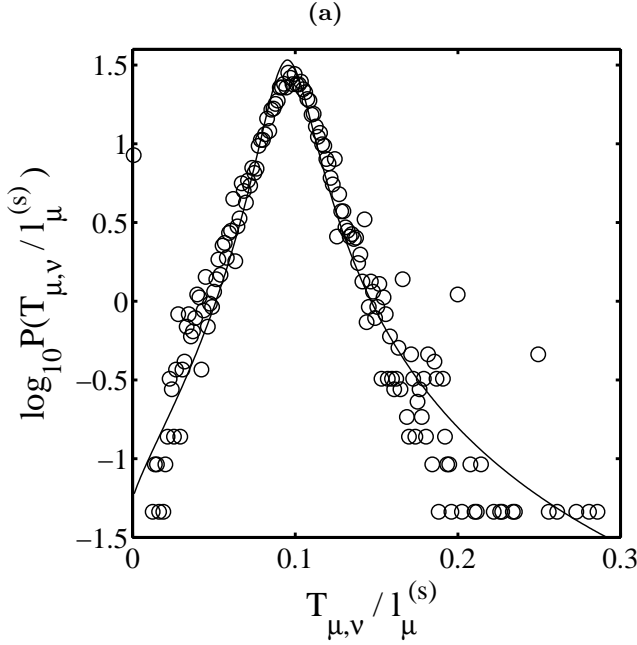


FIG. 10: Comparison of theory with measurements of average inter-tributary distances for the Scheidegger model. The data in both (a) and (b) is for the case of order  $\nu = 2$  side streams and order  $\mu = 6$  absorbing streams. In (a), the distribution of  $v = T_{\mu,\nu}/l_{\mu}^{(s)}$  obtained from the Scheidegger model (circles) is compared with the smooth curve predicted in equation (33). The same comparison is made for the reciprocal variable  $w = l_{\mu}^{(s)}/T_{\mu,\nu}$ , the predicted curve being given in equation (34).

Finally, we quantify how changes in the orders  $\mu$  and  $\nu$  affect the width of the distributions by considering some natural rescalings. Figure 11(a) shows binned, normalized distributions of  $T_{\mu,\nu}/l_{\mu}^{(s)}$  for the Scheidegger model. Here, the side stream order is  $\nu = 2$  and the absorbing stream orders range over  $\mu = 5$  to  $\mu = 8$ . All distributions are centered around  $\rho_2 \simeq 0.10$ .

Because the average length of  $l_{\mu}^{(s)}$  increases by a factor  $R_{l^{(s)}}$  with  $\mu$ , the typical number of side streams increases by the same factor. Since we can decompose  $l_{\mu}^{(s)}$  as

$$l_{\mu}^{(s)} = l_{\mu,\nu}^{(s,b)} + l_{\mu,\nu}^{(s,i)} + \dots + l_{\mu,\nu}^{(s,i)} + l_{\mu,\nu}^{(s,e)}, \quad (35)$$

where there are  $T_{\mu,\nu} - 1$  instances of  $l_{\mu,\nu}^{(s,i)}$ ,  $l_{\mu}^{(s)}$  becomes better and better approximated by  $(T_{\mu,\nu} + 1)\langle l_{\mu,\nu}^{(s,i)} \rangle$ .

Hence, the distribution of  $T_{\mu,\nu}/l_{\mu}^{(s)}$  peaks up around  $\rho_2$  as  $\mu$  increases, the typical width reducing by a factor of  $1/\sqrt{R_{l^{(s)}}}$  for every step in  $\mu$ . Using this observation, Figure 11(b) shows a rescaling of the same distributions shown in Figure 11(a). The form of this rescaling is

$$P(T_{\mu,\nu}/l_{\mu}^{(s)}) = (R_{l^{(s)}})^{\mu/2} G_1 \left( [T_{\mu,\nu}/l_{\mu}^{(s)} - \rho_2] (R_{l^{(s)}})^{\mu/2} \right) \quad (36)$$

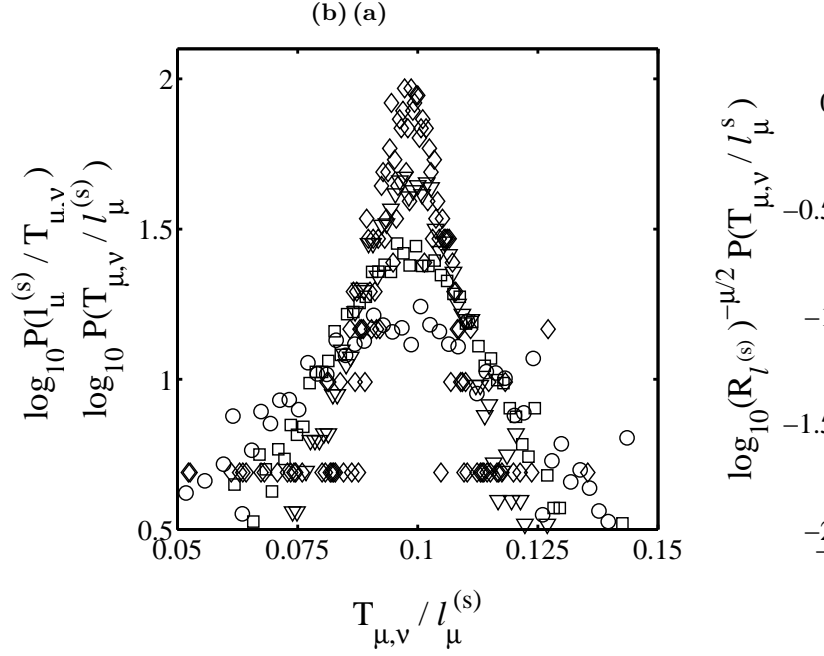


FIG. 11: Distributions of the quantity  $T_{\mu,\nu}/l_{\mu}^{(s)}$  for the Scheidegger model with  $\mu$ , the order of the absorbing stream, varying and the side stream order fixed at  $\nu = 2$ . Given in (a) are unrescaled distributions for  $\mu = 5$  (circles),  $\mu = 6$  (squares),  $\mu = 7$  (triangles), and  $\mu = 8$  (diamonds). Note that as the order of the absorbing stream increases so does its typical length. This leads to better averaging and the standard deviation of the distribution decays as  $R_{l^{(s)}}^{-\omega/2}$ . The distributions are all centered near the typical density of order  $\nu = 2$  side streams,  $\rho_2 \simeq 0.10$ . The rescaled versions of these distributions are given in (b) with the details as per equation (36).

where the function is similar to the form of  $P(v)$  given in equation (33). The mean drainage density of  $\rho_2$  has been subtracted to center the distribution.

We are able to generalize this scaling form of the distribution further by taking into account side stream order. Figures 12(a) and 12(b) respectively show the unrescaled and rescaled distributions of  $T_{\mu,\nu}/l_{\mu}^{(s)}$  with  $\nu$  allowed to vary. This particular example taken from the Scheidegger model is for  $\mu = 6$  and the range  $\nu = 1$  to  $\nu = 5$ . Since  $\nu$  is now changing, the centers are situated at the separate values of the  $\rho_{\nu}$ . Also, the typical number of side streams changes with order  $\nu$  so the widths of the distributions dilate as for the varying  $\mu$  case by a factor  $\sqrt{R_{l^{(s)}}}$ . Notice that the rescaling works well for  $\nu = 2, \dots, 5$  but not  $\nu = 1$ . As we have noted, deviations from scaling from small orders are to be expected. In this case, we are led to write down

$$P(T_{\mu,\nu}/l_{\nu}^{(s)})(R_{l^{(s)}})^{-\nu/2} G_2 \left( [T_{\mu,\nu}/l_{\nu}^{(s)} - \rho_{\nu}] (R_{l^{(s)}})^{-\nu/2} \right) \quad (37)$$

where, again,  $G_2(z)$  is similar in form to  $P(v)$ .

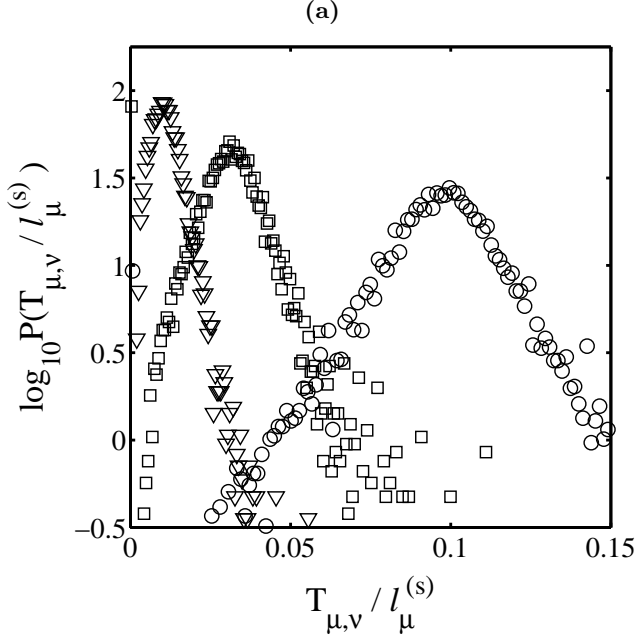


FIG. 12: Distributions of number of side streams per unit length for the Scheidegger model with  $\nu$ , the order of side streams, varying. For both (a) and (b), the absorbing stream order is  $\mu = 6$ . Shown in (a) are the unrescaled distributions for  $\nu = 2$  (circles),  $\nu = 3$  (squares), and  $\nu = 4$  (triangles). Note that as  $\nu$  increases, the mean number of side streams decreases as do the fluctuations. The distributions in (a) together with the distribution for  $\nu = 5$  (diamonds) are shown rescaled in (b) as per equation (38).

We find the same rescalings apply for the Mississippi data. For example, Figure 13(a) shows unrescaled distributions of  $T_{\mu,\nu}/l_{\nu}^{(s)}$  for varying  $\nu$ . Figure 13(b) then shows reasonable agreement with the form of equation (37). In this case, the Scheidegger model clearly affords valuable guidance in our investigations of real river networks. The ratio  $R_{l^{(s)}} = 2.40$  was calculated from an analysis of  $l_{\omega}^{(s)}$  and  $l_{\omega}$ . The density  $\rho_2 \simeq 0.0004$  was estimated directly from the distributions of  $T_{\mu,\nu}/l_{\nu}^{(s)}$  and means that approximately four second-order streams appear every ten kilometers.

Combining equations (38) and (38), we obtain the complete scaling form

$$P(T_{\mu,\nu}/l_{\nu}^{(s)}) = (R_{l^{(s)}})^{(\mu-\nu-1)/2} G\left([T_{\mu,\nu}/l_{\nu}^{(s)} - \rho_{\nu}]/(R_{l^{(s)}})^{(\mu-\nu-1)/2}\right) \quad (38)$$

As per  $G_1$  and  $G_2$ , the function  $G$  is similar in form to  $P(v)$ .

The above scaling form makes intuitive sense but is not obviously obtained from an inspection of (33). We therefore examine  $P(v)$  by determining the position and magnitude of its maximum. Rather than solve  $P'(v) = 0$  directly, we find an approximate solution by considering

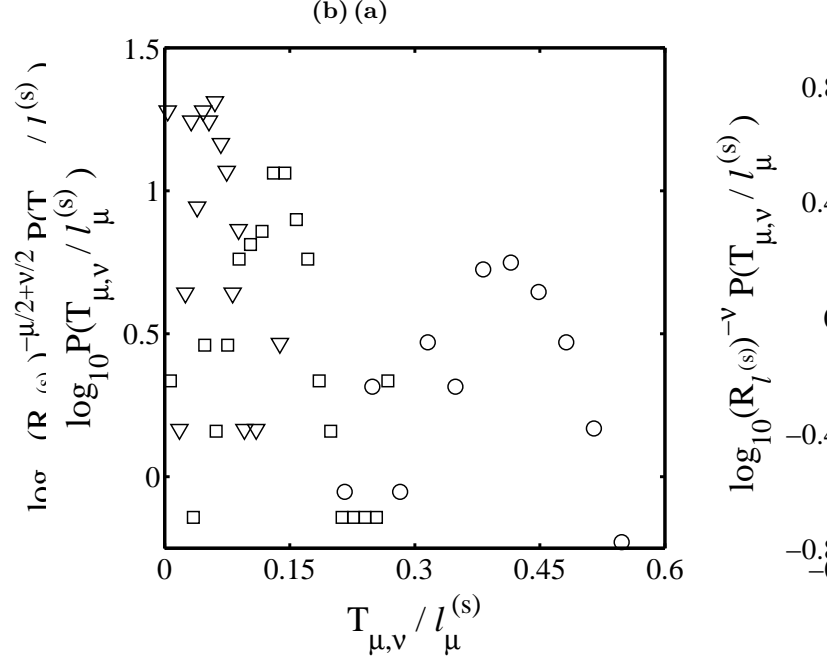


FIG. 13: Tokunaga statistics for the Mississippi river basin. The distributions are as per Figure 12(a), distributions of number of side streams per unit length with  $\nu$ , the order of side streams, varying. The absorbing stream order is  $\mu = 7$  and the individual distributions correspond to  $\nu = 2$  (circles),  $\nu = 3$  (squares) and  $\nu = 4$  (triangles). All lengths are measured in meters. Rescalings of the distributions shown in (a) along with that for  $\nu = 5$  (diamonds) are found in (b). Reasonable agreement with equation (38) is observed.

the argument of the denominator,  $-\ln F(v)$ , with  $F(v)$  given in equation (27). Since the numerator of  $P(v)$  is  $1 + v^2$  and the maximum occurs for small  $v$  this is a justifiable step. Setting  $dF/dv = 0$ , we thus have

$$-\ln \frac{1-v}{q} + \ln vp = 0, \quad (39)$$

which gives  $v_m = p/(q+p) = p/(1-\tilde{p})$ . Note that for  $\tilde{p} \ll 1$ , we have  $v_m \simeq p$ .

Substituting  $v = v_m = p/(1-\tilde{p})$  into equation (33), we find

$$P(v_m) \simeq N'' \tilde{p}^{-3/2} = N \tilde{p}^{-1/2} 2^{-3/2} \quad (40)$$

presuming  $p^2 \ll 1$  and  $q \simeq 1$ . Returning to the scaling form of equation (38), we see that the  $\tilde{p}^{-1/2}$  factor in equation (40) accounts for the factors of  $(R_{l^{(s)}})^{\mu/2}$  since  $\tilde{p} = \tilde{p}_{\mu}$  scales from level to level by the ratio  $R_{l^{(s)}}$ . We therefore find the other factor  $(R_{l^{(s)}})^{\nu/2}$  of equation (38) gives  $N = cp^{1/2}$  where  $c$  is a constant. Since  $p = p_{\nu}$ , it is the only factor that can provide this variation. We thus have found the variation with stream order of the normalization  $N$  and have fully characterized,  $P(x, y)$ , the continuum approximation of  $P(l_{\mu}^{(s)}, T_{\mu,\nu})$ .

## IX. CONCLUDING REMARKS

We have extensively investigated river network architecture as viewed in planform. We identify the self-similarity of a form of drainage density as the essence of the average connectivity and structure of networks. From previous work in [4], we then understand this to be a base from which all river network scaling laws may be obtained.

We have extended the description of tributary structure provided by Tokunaga's law to find that side stream numbers are distributed exponentially. This in turn is seen to follow from the fact that the length of stream segments are themselves exponentially distributed. We interpret this to be consequence of randomness in the spatial distribution of stream segments. Furthermore, the presence of exponential distributions indicate fluctuations in variables are significant being on the order of mean values. For the example of stream segment lengths, we thus identify  $\xi_{l^{(s)}}$ , a single parameter needed to describe all moments. This is simply related to  $\xi_t$ , which describes the distributions of Tokunaga ratios. The exponential distribution becomes the null hypothesis for the distributions of these variables to be used in the examination of real river networks.

We are able to discern the finer details of the connection between stream segment length and tributary numbers. Analysis of the placement of side streams along a stream segment again reveals exponential distributions. We are then able to postulate a joint probability distribution for stream segment lengths and the Tokunaga ratios. The functional form obtained agrees well with both model and real network data. By further considering distributions of the number of side streams per unit length of individual stream segments, we are able to capture how variations in the separation of side streams are

averaged out along higher-order absorbing streams.

By expanding our knowledge of the underlying distributions through empiricism, modeling and theory, we obtain a more detailed picture of network structure with which to compare real and theoretical networks. We have also further shown that the simple random network model of Scheidegger has an impressive ability to produce statistics whose form may then be observed in nature. Indeed, the only distinction between the two is the exact value of the scaling exponents and ratios involved since all distributions match up in functional form.

We end with a brief comment on the work of Cui *et al.* [13] who have recently also proposed a stochastic generalization of Tokunaga's law. They postulate that the underlying distribution for the  $T_{\mu,\nu}$  is a negative binomial distribution. One parameter additional to  $T_1$  and  $R_T$ ,  $\alpha$ , was introduced to reflect "regional variability," i.e., statistical fluctuations in network structure. This is in the same spirit as our identification of a single parameter  $\xi_t$ . However, our work disagrees on the nature of the underlying distribution of  $T_{\mu,\nu}$ . We have consistently observed exponential distributions for  $T_{\mu,\nu}$  in both model and real networks.

In closing, by finding randomness in the spatial distribution of stream segments, we have arrived at the most basic description of river network architecture. Understanding the origin of the exact values of quantities such as drainage density remains an open problem.

## Acknowledgements

The authors would like to thank J.S. Weitz for useful discussions. This work was supported in part by NSF grant EAR-9706220 and the Department of Energy grant DE FG02-99ER 15004.

- 
- [1] P. S. Dodds and D. H. Rothman, *Geometry of River Networks I: Scaling, Fluctuations, and Deviations* (2000), submitted to PRE.
  - [2] A. Maritan, A. Rinaldo, R. Rigon, A. Giacometti, and I. Rodríguez-Iturbe, *Phys. Rev. E* **53**(2), 1510 (1996).
  - [3] I. Rodríguez-Iturbe and A. Rinaldo, *Fractal River Basins: Chance and Self-Organization* (Cambridge University Press, Great Britain, 1997).
  - [4] P. S. Dodds and D. H. Rothman, *Phys. Rev. E* **59**(5), 4865 (1999), cond-mat/9808244.
  - [5] P. S. Dodds and D. H. Rothman, *Annu. Rev. Earth Planet. Sci.* **28**, 571 (2000).
  - [6] P. S. Dodds and D. H. Rothman, *Geometry of River Networks II: Distributions of Component Size and Number* (2000), submitted to PRE.
  - [7] E. Tokunaga, *Geophys. Bull. Hokkaido Univ.* **15**, 1 (1966).
  - [8] E. Tokunaga, *Geogr. Rep., Tokyo Metrop. Univ.* **13**, 1 (1978).
  - [9] E. Tokunaga, *Trans. Jpn. Geomorphol. Union* **5**(2), 71 (1984).
  - [10] A. E. Scheidegger, *Bull. Int. Assoc. Sci. Hydrol.* **12**(1), 15 (1967).
  - [11] R. E. Horton, *Bull. Geol. Soc. Am* **56**(3), 275 (1945).
  - [12] A. N. Strahler, *EOS Trans. AGU* **38**(6), 913 (1957).
  - [13] G. Cui, B. Williams, and G. Kuczera, *Water Resour. Res.* **35**(10), 3139 (1999).
  - [14] D. L. Turcotte, J. D. Pelletier, and W. I. Newman, *J. Theor. Biol.* **193**, 577 (1998).
  - [15] S. D. Peckham, *Water Resour. Res.* **31**(4), 1023 (1995).
  - [16] S. A. Schumm, *Bull. Geol. Soc. Am* **67**, 597 (1956).
  - [17] J. S. Huxley and G. Teissier, *Nature* **137**, 780 (1936).
  - [18] J. T. Hack, *U.S. Geol. Surv. Prof. Pap.* **294-B**, 45 (1957).
  - [19] F. Colaiori, A. Flammini, A. Maritan, and J. R. Banavar, *Phys. Rev. E* **55**(2), 1298 (1997).
  - [20] D. G. Tarboton, R. L. Bras, and I. Rodríguez-Iturbe, *Water Resour. Res.* **26**(9), 2243 (1990).
  - [21] S. S. Manna, D. Dhar, and S. N. Majumdar, *Phys. Rev. A* **46**, 4471 (1992).
  - [22] S. S. Manna and B. Subramanian, *Phys. Rev. Lett.*

- 76**(18), 3460 (1996).
- [23] W. Feller, *An Introduction to Probability Theory and Its Applications*, vol. I (John Wiley & Sons, New York, 1968), third ed.
- [24] H. Takayasu, I. Nishikawa, and H. Tasaki, *Phys. Rev. A* **37**(8), 3110 (1988).
- [25] M. Takayasu and H. Takayasu, *Phys. Rev. A* **39**(8), 4345 (1989).
- [26] H. Takayasu, M. Takayasu, A. Provata, and G. Huber, *J. Stat. Phys.* **65**(3/4), 725 (1991).
- [27] G. Huber, *Physica A* **170**, 463 (1991).
- [28] D. Dhar, *Physica A* **263**, 4 (1999).
- [29] C. M. Bender and S. A. Orszag, *Advanced mathematical methods for scientists and engineers*, International series in pure and applied mathematics (McGraw-Hill, New York, 1978).
- [30] The network for the Mississippi was extracted from a topographic dataset constructed from three arc second USGS Digital Elevation Maps, decimated by averaging to approximately 1000 meter horizontal resolution ([www.usgs.gov](http://www.usgs.gov)). At this grid scale, the Mississippi was found to be an order  $\Omega = 11$  basin.